Results in Materials 6 (2020) 100088

Contents lists available at ScienceDirect

Results in Materials

journal homepage: www.journals.elsevier.com/results-in-materials

Controlling electrical and optical properties of zinc oxide thin films grown by thermal atomic layer deposition with oxygen gas

Tai Nguyen [a,b], Noureddine Adjeroud [a], Mael Guennou [b], Jérôme Guillot [a], Yves Fleming [a], Anne-Marie Papon [c], Didier Arl [a], Kevin Menguelti [a], Raoul Joly [a,b], Narciso Gambacorti [c], Jérôme Polesel-Maris [a,*]

[a] Materials Research and Technology Department, Luxembourg Institute of Science and Technology, 41, Rue Du Brill, L-4422, Belvaux, Luxembourg
[b] Physics and Materials Science Research Unit, University of Luxembourg, Campus Limpertsberg, 162 Avenue de La Faïencerie, L-1511, Luxembourg
[c] Univ. Grenoble Alpes, CEA, LETI, F-38000, Grenoble, France

ARTICLE INFO

Keywords:
Zinc oxide thin film
Atomic layer deposition
Oxygen chemisorption
Polar surface stabilization
Electrical properties
Optical properties

ABSTRACT

The preparation of ZnO thin films with controlled electrical resistivity and optical properties is often challenged by the presence of defects, such as oxygen vacancies or interstitial zinc. Here, we investigate the material properties of ZnO polycrystalline thin films prepared by thermal Atomic Layer Deposition (ALD) with the presence of molecular oxygen pulsing during the growth. By means of structural, electrical and optical characterizations, we identify key growth parameters of this unusual ALD process. Unexpectedly, the influence of oxygen molecules on the crystallography, microstructure and morphology of ZnO films is significant from hundred-nanometers to micrometer thick film. The electrical resistivity of the films grown with oxygen gas shows a dramatic increase from 3 to 4 orders of magnitude. Additionally, photoluminescence measurements reveal that deep-level emissions caused by defects located deep in the band gap can be reduced by applying an adequate pulsing of oxygen gas during the process. Finally, we conclude with a discussion about the degree of consistency between the chemical composition, the inner strain and the optical and electrical properties of the films obtained with the different thermodynamic parameters of growth. Several hypotheses are discussed in order to understand the dominance of (002) orientation in the presence of oxygen during the ALD growth process.

1. Introduction

The control of surface morphology and preferred crystallographic orientation has played an essential role in ensuring and upgrading the performance of electronic devices based on zinc oxide thin films [1]. Wurtzite hexagonal zinc oxide has attracted considerable attention due to its excellent properties for transparent electronics, such as a wide direct band gap of 3.37 eV [1,2], large exciton binding energy of 60 meV [3], but also for MEMS actuators with its piezoelectric properties [4]. Therefore, they have been found in vast applications from UV light emitting diodes (LED) [5], flat panel displays [6], and solar cells [7] to gas sensors [8,9], surface acoustic wave devices (SAW) [10], and nano-generators [11–14]. The properties of zinc oxide thin films strongly depend on their surface morphology and crystallographic structures, and therefore, processing efforts are required for them to fit specific applications. For instance, the non-polar *m*-plane (100) and *a*-plane (110) of ZnO crystals are beneficial for high-efficiency LED and transparent conductive oxide applications [15,16], whereas polar *c*-plane (002) ZnO thin films are employed for potential applications containing sensors [17], nanogenerators [13], piezotronics [18–22], and energy harvesters [23], due to the spontaneous and piezoelectric polarization effects along the *c*-axis [1].

For piezoelectric-based applications, ZnO thin films are required to give preferred (002) orientation and high resistivity (or low leakage current) to ensure the highest output voltages. Several fabrication methods have been reported to achieve polar-plane (002) ZnO thin films, including low gas pressure [24] or control of the $Ar:O_2$ ratio in sputtering [25], high substrate temperatures and an oxygen-rich environment in pulsed laser deposition (PLD) [26], plasma-enhanced chemical vapor deposition (PECVD) [27], and atomic layer deposition (ALD) [28]. Among these techniques, ALD has emerged as a suitable method for the synthesis of high quality, (002)-oriented and highly conformal thin films

* Corresponding author.
E-mail address: jerome.polesel@list.lu (J. Polesel-Maris).

https://doi.org/10.1016/j.rinma.2020.100088
Received in revised form 14 January 2020; Accepted 20 February 2020
Available online 2 April 2020

with low structural-defect density. Additionally, the relatively low temperatures of the ALD processes are compatible with both inorganic and fragile organic substrates. In an ALD process using diethylzinc (DEZ) and water as precursors, the non-polar (100) orientation dominates at low temperatures between 100 °C and 250 °C. Conversely, the polar (002) preferred orientation can only be observed at relatively elevated temperatures for ALD, above 250 °C [28,29].

Recently, M. A. Thomas et al. [30] have reported that using oxygen radicals produced during ALD processes can strongly affect the surface morphology, crystallite structure and electrical properties of the ZnO thin films at temperatures as low as 200 °C. In their work, the ZnO thin films were grown with DEZ and water as precursors, and the films were treated *in situ* by oxygen plasma after each cycle–a method called plasma enhanced thermal ALD (PET-ALD). They have observed a giant enhancement of resistivity (about seven orders of magnitude) of the PET-ALD ZnO films compared to simple ALD films without oxygen plasma treatment, and have attributed it to a lower concentration of oxygen vacancies as a result of their neutralization by oxygen radicals after the plasma treatment. They suggested that the ethyl ligands from DEZ can be further cleaved/combusted by energetic oxygen radicals, thus modifying the morphological and crystalline structures. However, the growth mechanism of the preferred (002) orientation has not been clarified in detail. R. Huang et al. [31] have applied *in situ* plasma O_2 treatment after each DEZ – water ALD cycle to highlight the possibility of modulating the ZnO film resistivity and the Fermi level. However, the supercycled ALD processes they proposed were found to barely influence the crystalline orientation. Only S. Park and Y. Lee [32] reported the use of oxygen gas after each cycle of DEZ and water to grow ZnO thin films by thermal ALD without any plasma enhancement. The presence of a molecular oxygen pulse during the ALD process of ZnO profoundly influenced the film morphologies, the crystalline structures, and the electrical properties. The film crystallite modified robustly from nonpolar (100) preferred orientation to polar (002) preferred orientation, and the resistivity of the films increased by two orders of magnitude. Nevertheless, open questions remain about the growth mechanisms, the reason for the significant increase of the electrical resistivity, and the influence of this process on other physical properties like strain or optical absorption.

In the present study, we have systematically investigated the effects of oxygen gas introduced during thermal ALD processes on the ZnO thin film properties by varying the thermodynamic growth parameters. We varied the pulsing time of the molecular oxygen introduced during the process and the substrate temperature separately. The results obtained suggest that by applying the relevant oxygen pulse time and substrate temperature, the crystallographic structure of ZnO films can be highly controlled from random orientations to the preferentially polar orientation. Moreover, due to uncommon treatment by oxygen molecules during the ALD growths, not only electrical and optical properties but also the electronic properties are significantly impacted, as proven by novel characterizations such as four-point probe, UV–visible optical spectroscopy, photoluminescence measurements, and x-ray photoelectron spectrometry. The dramatic increase of the electrical resistivity from 3 to 4 orders of magnitude is expected for improving current leakage issues in the piezoelectric applications of ZnO thin films as actuators or strain sensors. Additionally, the photoluminescence measurements reveal that deep-level emissions caused by defects located deep in the band gap can be reduced. This would have a positive impact on the UV light emission efficiency of ZnO devices like LED. Subsequently, based on those results, the possible growth mechanisms and rational interpretations for the significant increases of resistivity, as well as correlations of the structural, optical and electronic properties of ZnO films are discussed.

2. Experimental details

The ZnO thin films were synthesized using standard precursors, such as diethylzinc [DEZ, $Zn(C_2H_5)_2$] (Strem Chemicals, Inc., France), deionized (DI) MilliQ water (resistivity of 18.2 MΩ cm at 25 °C), and O_2 gas (stand-alone bottle, Air Liquide, alpha 2 O_2 global purity ≥ 99.9995% mol with less than 0.5H_2O ppm. mol impurity) in a commercial atomic layer deposition reactor (TFS-200, Beneq, Finland). The Argon gas used for purging during the ALD process was ALPHAGAZ™ 2 with a global purity of ≥99.9999% mol with less than 0.5H_2O ppm. mol impurity. The supporting surfaces for the ZnO thin film deposition were 2 × 2 cm^2 pieces of single crystal Si(100) wafer (Siegert GmbH, Germany, grade Monitor), pristine and coated by sputtering (Bal-Tec Med 020 high vacuum coating system) with a 150-nm layer of nickel (target purity level of 99.999%, reference NI000565, Goodfellow GmbH, Germany) and glass slides (Thermo Scientific, Germany). Prior to the synthesis of ZnO thin films, the substrates were cleaned in acetone, isopropanol, DI water and dehydrated for 20 min at 200 °C. Just before introduction into the ALD reactor, an additional plasma cleaning (Plasma Therm 790 RIE, 120 W, 10 min, in Ar:O_2 gases environment at 30 mTorr) was performed on the substrates. The ZnO thin films were elaborated without using molecular oxygen gas at a substrate temperature of 180 °C by the following four-step sequence: DEZ pulse (0.1 s), Ar purge (5 s), DI water pulse (0.1 s), and Ar purge (5 s). In contrast, when using oxygen gas pulsing, the ZnO thin films were deposited at 180 °C by a sequence of six pulses; DEZ pulse (0.1 s), Ar purge (5 s), O_2 pulse, Ar purge (20 s), DI water pulse (0.1 s), and Ar purge (10 s), where the pulsing time of oxygen gas varied between 1, 3, and 5 s. The temperature-dependent studies were performed using the sequence of six pulses at substrate temperatures of 100, 150, 180, and 200 °C with a constant oxygen pulsing time of 1 s. The ZnO thin films were deposited by 500 cycles for all studies, except for the films studied by cross-section transmission electron microscopy (TEM) with 5000 cycles, which were set to achieve a thicker layer of about 1 μm. Before processes implying either DEZ/H_2O or DEZ/O_2/H_2O precursors, we performed zinc oxide deposition tests by using DEZ and O_2 as precursors for Zn and O, respectively. No film was formed [32] (not detectable by ellipsometry) at a temperature of 180 °C, confirming the global purity of the O_2 gas source from moisture contamination. We also did the same quality control of the Argon gas by pulsing only the DEZ precursor in the same conditions, and no film was formed, thus also confirming the global purity of the Ar gas source in the ALD reactor.

X-ray diffractometry (Diffractometer Bruker D8 Discover with Cu Kα radiation and a 5-axis Eulerian cradle) was conducted in θ–2θ (Bragg-Brentano) and in grazing incidence (ω = 0.5°) (GIXRD) configurations to estimate the crystalline quality of the ZnO thin films on all samples. The measurement uncertainty in angle 2θ was estimated to 0.02°, based on repetitive measurements following the sample alignment. For pole figures, the measurements were performed in θ–2θ mode with a measurement in increments of 5° in ϕ (phi) and 3° in χ (chi). The measurement was performed up to 72° in χ. The pole figures were performed using collimated irradiation of 1 mm beam diameter. For both samples, pole figures were performed on the (100), (002) and (101) peak positions. For each peak position, the background was measured to the right and the left of the peak position for one angle of phi only. The defocussing correction was performed based on the number of counts measured on the (104) and (113) peak positions of the NIST standard SRM1976. The pole figure data treatment measured was performed using the MTEX toolbox (version 5.1.1) [33] in conjunction with Matlab ®. The microstructure of samples was analyzed by scanning electron microscopy (SEM) on a Helios Nanolab 650 FIB-SEM instrument (FEI Company, USA). Cross-sectional configurations were carried out to further confirm the thickness of the ZnO thin films measured by ellipsometry using a J.A. Woollam M2000 instrument (analysis wavelength 300–1000 nm) with three different angles 65, 70, and 75°. The growth rate was calculated as the ratio of the thickness of the ZnO layer over the number of ALD loops. TEM analysis in cross section and diffraction were performed on a JEOL 3010F microscope operating at 300 kV. The instrument has a 0.17 nm atomic resolution. A four-point probe and Hall measurements (Ecopia HMS-3000) were performed to measure the resistivity and carrier concentration of the thin film samples on glass substrates, respectively. Elemental composition and chemical states were studied by x-ray

photoelectron spectrometry (XPS) (Axis Ultra DLD, Kratos Analytical Ltd.) using an x-ray source (Al K_α monochromated, E = 1486.6 eV) at a power of 150 W, and an energy resolution of 1.5 eV for survey scans and 0.55 eV for narrow scans determined on a silver sample. The surface area analyzed was 110 μm × 110 μm. The spectra have been calibrated in energy from the Zn 2p peak in ZnO at 1022.0 eV. The depth profiles were carried out in the 3 mm × 3 mm etched area by an Ar^+ ion beam operating at 2 kV and 2 μA. The UV–visible measurements (LAMBDA 1050 UV/Vis Spectrophotometer, PerkinElmer) were conducted in a 250-2000 nm-range wavelength to measure the transmittance and reflection spectra of ZnO thin films on glass slides. Photoluminescence (PL) measurements were carried out at room temperature in a Renishaw inVia confocal micro-Raman spectrometer, with an excitation wavelength of 325 nm provided by an 8 mW He–Cd laser focused through a Thorlabs UV objective with 40× magnification and a numerical aperture of 0.5. A 300 gr/mm grating enabled analysis in the 350–900 nm range. The PL spectrum was normalized in intensity for the sake of clarity of comparison between each sample analysis. A hexagonal <0001>-oriented ZnO single crystal purchased from MTI Corporation was characterized and taken as a reference spectrum.

3. Results

3.1. Effect of the pulsing time of oxygen

3.1.1. Structural and morphological properties

Fig. 1(a) illustrates the growth rate of ZnO thin films for varying pulsing times of oxygen for a constant substrate temperature of 180 °C. The growth rate of the ZnO films decreased significantly and stabilized with increasing pulsing times: it was about 2.48, 1.82, 1.67, and 1.69 Å/cycle for films grown with oxygen gas pulsing times of 0, 1, 3, and 5 s, respectively.

Fig. 1(b) presents the grazing incident x-ray diffraction (GIXRD) for four nickel-coated samples. For all ZnO samples, the diffraction patterns match well with the standard diffraction patterns of the wurtzite ZnO crystal structure (JCPDS-36-1451). ZnO thin films grown without oxygen gas displayed a contribution from three different diffraction peaks, i.e. the (100), (002) and (101) orientations. On the other hand, for ZnO thin films grown in the presence of oxygen gas, the (002) diffraction peak, which is characteristic of the polar plane, becomes dominant, and the (100) and (101) diffraction peaks are reduced to tiny peaks located around 31.77° and 36.22°, respectively (Fig. 1(b)). This indicates that these films grow preferentially along the c-axis.

In order to quantify the preferred (002) orientation of the ZnO films, we defined a Grazing Incidence Texture Coefficient (GI-TC) for the *hkl* plane, as shown by the following equations:

$$\mathrm{GI-TC}(hkl) = \frac{I_r(hkl)}{N^{-1}\sum_N I_r(hkl)} \quad (1)$$

and

$$I_r(hkl) = I_{(hkl)} / I^0_{(hkl)} \quad (2)$$

where $I_{(hkl)}$ are the relative intensities of (hkl) peaks measured on the thin film samples, $I^0_{(hkl)}$ corresponds to the relative intensity for the same reflection on an isotropic randomly oriented ZnO powder (NIST Standard SRM674B) measured in exactly the same configuration, and N is the number of Bragg reflections considered. Here, N = 3 because we investigated the orientations (100), (002), and (101). This expression of the GI-TC, although close to the TC definition found in Ref. [34,35], cannot be assimilated to it since we performed the measurement at grazing incidence, with the same incident angle for all samples, and not in θ-2θ mode. By construction, as for TC, the GI-TC is 1 for a non-textured sample and has a value of N for single oriented crystals.

To verify that the ZnO powder really is isotropic and randomly oriented, a measurement was performed in θ-2θ mode and compared to the reference pattern in the JCPDS database. As shown in Fig. S2 in the Supporting Information, the Texture Coefficient (TC) of the three Bragg peaks (100), (002), and (101), as defined in Refs. [34,35] were almost exactly 1, confirming that the powder really was isotropic and randomly oriented and consequently could be used as a reference pattern.

The GI-TC values of the ZnO thin films on nickel-coated silicon substrates, which are shown in Table 1, clearly confirmed that the strong domination of (002) crystal orientation outweighs the (100) and (101) orientations in the ZnO thin films grown with oxygen gas (see Fig. S3, Supporting Information). In addition, the GI-TC (002) of the ZnO film grown with 1-s oxygen gas pulsing shows the highest value in comparison to the other samples. This implies a highly preferred orientation along the c-axis for this sample.

The pole figures shown in Fig. 3 give complementary information about the preferred orientation of the ZnO grains in the polycrystalline film grown without [Fig. 3(a)] and with [Fig. 3(b)] the presence of molecular oxygen pulsing (1 s) at a sample temperature of 180 °C. The calculated Orientation Distribution Functions (ODF) deduced from the measured pole figures show that indeed some degree of texture is present on both samples. Thus, the pole figures of the ZnO film grown with the presence of molecular oxygen pulsing [Fig. 3(b)] present a preferred orientation along the c-axis without any significant misalignment. It can be seen that the (002) orientation (along the c-axis) is significantly more pronounced in the ZnO thin film grown with the presence of the oxygen gas. This change in texture is confirmed by the calculated texture index/entropy [36] changing from 2.42/-0.43 for the ZnO film grown without the O_2 gas (Fig. 3(a)) to 6.89/-1.34 for the ZnO grown with the O_2 gas

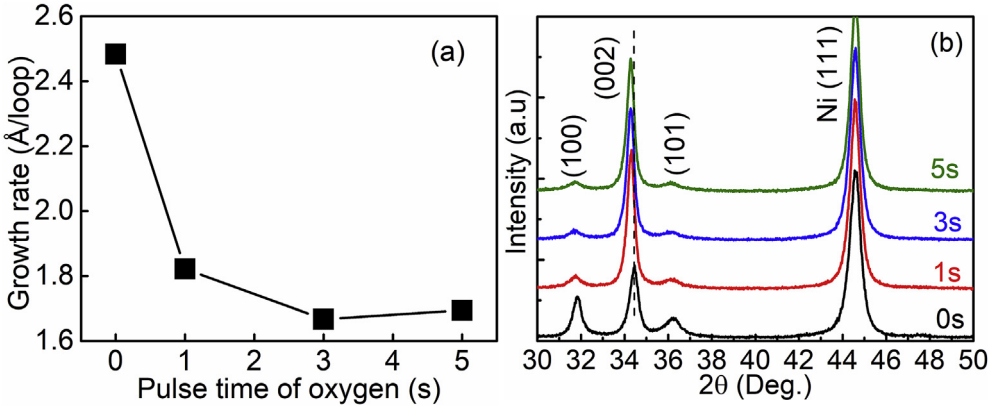

Fig. 1. (a) Growth rate, and (b) grazing incidence x-ray diffraction pattern (ω = 0.5°) of ZnO thin films grown at 180 °C with different oxygen pulsing times. The nickel (111) peak was used as a reference to track the shift of the diffraction peaks of ZnO films. The black dashed vertical line highlights the shift of the (002) peak.

Table 1
Sample references, thicknesses, lattice constants, induced intrinsic strain, grazing incidence texture coefficient, oxygen over zinc ratio (O/Zn), and photoluminescence intensity ratio (I_{NBE}/I_{DLE}) of ZnO thin films processed with different pulsing times of oxygen and substrate temperatures.

Sample	Thickness (nm)	a(Å)	c (Å)	Strain (%) [a]	|ΔStrain| (%) [b]	$\|\Delta Strain\|_{thickness}$ (%) [c]	GI-TC [d]			O/Zn ratio	I_{NBE}/I_{DLE}
							(100)	(002)	(101)		
0 s	124.2	3.237	5.193	−0.345			0.86	1.87	0.27	0.92 ± 0.02	1.81
1 s	91.1	3.241	5.216	0.096	0.441	0.105	0.25	2.63	0.12	0.96 ± 0.03	17.24
3 s	83.4	3.249	5.218	0.134	0.038	0.024	0.22	2.67	0.11	0.93 ± 0.03	4.70
5 s	84.7	3.245	5.220	0.173	0.039	0.004	0.20	2.68	0.12	0.95 ± 0.04	3.98
100 °C	72.6	3.251	5.225	0.269			1.06	1.59	0.34	0.98 ± 0.04	1.94
150 °C	84.2	3.251	5.221	0.192	0.077	0.037	0.47	2.33	0.20	0.95 ± 0.04	5.25
180 °C	91.1	3.241	5.216	0.096	0.096	0.022	0.25	2.63	0.12	0.96 ± 0.03	17.24
200 °C	103.6	3.237	5.201	−0.192	0.288	0.040	0.26	2.61	0.13	0.95 ± 0.04	2.85
Ref.[e]	–	3.253	5.211	–			–	–	–	–	18.06

[a] Strain is calculated by $\varepsilon = \frac{c - c_0}{c_0}$ with $c_0 = 5.211$ Å.

[b] Absolute strain change calculated as $|\varepsilon_{n-1} - \varepsilon_n|$ from the previous strain column. n is the row index in the table.

[c] Absolute strain change induced by thickness change calculated as $|\varepsilon_{n-1} - \varepsilon_n|$ from the thickness column, according to T. Singh et al. [64].

[d] Grazing incidence Texture Coefficient GI-TC (see Figs. S3 and S4 in the Supporting Information).

[e] References: 1) The ZnO reference (JCPDS-36-1451) is used for the lattice parameters a and c; 2) hexagonal <0001>-oriented ZnO single crystal purchased from MTI Corporation was used for the photoluminescence intensity ratio (I_{NBE}/I_{DLE}).

[Fig. 3(b)]. The change in texture is also reflected in the measured TC and GI-TC shown in Figs S2, S3 and S4 (Supporting Information), where the value of the (002) reflection is close to 3 for the sample grown with the presence of molecular oxygen pulsing (1 s) at a sample temperature of 180 °C.

Furthermore, a remarkable shift of the (002) diffraction peak of ZnO thin films fabricated under different pulsing times of oxygen gas was observed. Here, zinc oxide thin films were deposited on nickel-coated silicon substrates, but we observed the same tendency when they were deposited on a glass sample as shown in Fig. S1 in the Supporting Information. For all the samples, the diffraction peak of nickel (111) was located at the same position (around $2\Theta = 44.59°$) before and after ALD processes ramping up from 100 °C to 200 °C, and was used as a reference to track the shift of the ZnO (002) peak considered. Therefore, a shift in the (002) diffraction peak for the ZnO layer was an intrinsic effect due to the presence of oxygen gas during ALD processes. The positions of the (002) diffraction peak is noted in Table 1. It was around 34.5° for a ZnO thin film fabricated without using oxygen gas. By introducing oxygen gas during the process, it shifted markedly to lower angles. The (002) peak positions were 33.34, 33.33 and 33.32° for ZnO films with oxygen gas pulsing times of 1, 3, and 5 s, respectively. The ZnO reference (JCPDS-36-1451) gives a value of about 34.38° for the (002) peak position. In comparison to the peak position referenced for wurtzite ZnO in the database, the (002) diffraction peak on the ZnO thin film without oxygen gas was located at a higher angle, whereas that of the ZnO thin film using oxygen gas is located at lower angles. The lattice parameters a and c of the wurtzite hexagonal structure ZnO were calculated by using Bragg's law (cf. detailed expression in the supporting information) and their values for all films are listed in Table 1. It showed that the strain state of ZnO films changed from compressive to tensile for ZnO films with an increasing O_2 pulsing time. In the case of tensile strain, the unit cells of ZnO were elongated along the c-axis, while they slightly shrunk along the a-axis.

Top-view SEM micrographs of ZnO thin films are shown in Fig. 2. It can be seen in Fig. 2(a) that the ZnO thin film grown without using oxygen gas clearly shows a distribution of different grain orientations with

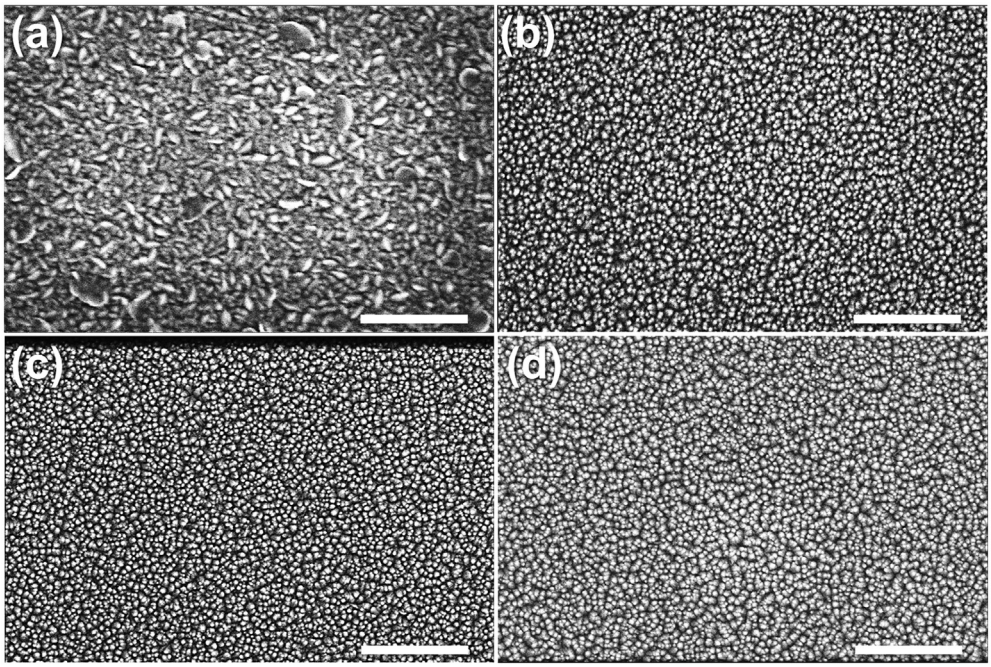

Fig. 2. SEM top view micrographs of ZnO thin films grown at 180 °C with an oxygen pulsing time of (a) 0 s, (b) 1 s, (c) 3 s, and (d) 5 s. The scale bar is 300 nm.

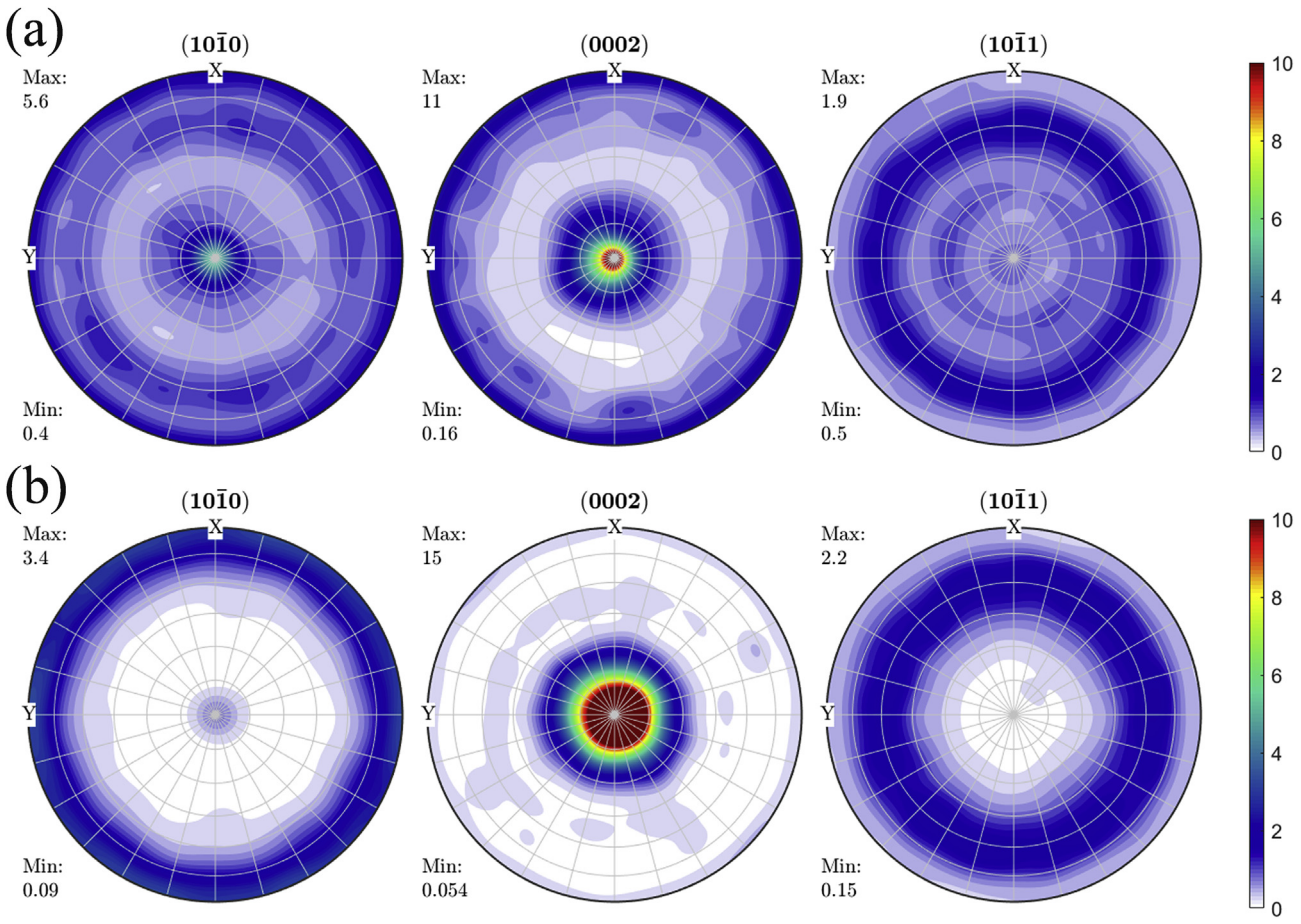

Fig. 3. Calculated Orientation Distribution Functions (ODF) from XRD pole figures of ZnO thin film deposited at 180 °C a) without and b) with the presence of O_2 gas pulses during the ALD growth. In this figure, the depicted poles are denoted using the Bravais-Miller notation (h k i l) with h + k + i = 0. The corresponding measured pole figures are shown in Figs. S5 and S6 in the Supporting Information document.

wedge-like shaped crystallites parallel to the substrate and fine-columnar crystallites perpendicular to the substrate. It is consistent with the x-ray diffraction data that shows a mixture of (100), (002), and (100) orientations. Fig. 2(b)-2(d) present the top-view SEM micrographs of ZnO thin films processed with oxygen. Interestingly, a significant change in the morphologies of those films can be observed, in that they are composed of grains which are mostly vertically oriented along the (002) direction (see Fig. S7 in the Supporting Information). Finally, we did not observe any significant difference between ZnO films grown with different pulsing times of oxygen gas; all exhibit the same morphology and have comparable grain diameters (from 12 to 18 nm).

We investigated the evolution of the grain structure and size distribution by cross section and diffraction TEM on a thicker ZnO layer of 1 μm for the growth process without (Fig. 4) and with (Fig. 5) the presence of molecular oxygen pulsing (1 s) at a sample temperature of 180 °C. Similarly to the previous results, both were performed on a nickel bottom layer. At the end of the process, a top capping layer of aluminum nitride (AlN) was also applied by ALD in the same reactor. The cross section micrographs in Fig. 4(a) highlight a rough polycrystalline ZnO layer of 1.14 μm thickness with a widening of grain sizes from 20 nm at the bottom to 100 nm on top. For 5000 ALD cycles, the growth rate is of 2.28 Å/cycle and the film roughness was estimated to about 120 nm. The detailed view [Fig. 4(b)] of the bottom part of the cross section confirmed small diameter grains from 20 to 30 nm. The TEM diffraction pattern [Fig. 4(c)] shows the <011> pole orientation of the monocrystalline silicon substrate with (111), (200), (022) intense spots and the main ring peak of the (111) orientation of the nickel bottom layer, and for the ZnO layer, weak ring peaks without preferential orientation. The cross-section micrographs in Fig. 5(a) highlight a regular (002) textured ZnO layer of 0.97 μm thickness with a regular preferential orientation of columnar grains with a constant diameter of 40 nm from bottom to top. For the same number of 5000 ALD cycles, the growth rate is reduced to 1.94 Å/cycle in agreement with the previous tendency observed in Fig. 1(a). In addition, the ZnO film roughness was about 30 nm. The TEM diffraction pattern [Fig. 5(b)] clearly revealed an intense peak for ZnO relative to a highly preferential (002) orientation, that is a (002) ZnO spot in a small arc shaped parallel to (200) Si, the normal direction to the substrate. Thus, columnar ZnO grains are similar to monocrystalline grains with their normal direction close to (002) parallel to (200) Si. The same previous diffraction peaks occur for the silicon substrate and the nickel bottom layer with the (111) ring peak. We performed the same ALD recipes for ZnO growth on an AlN bottom seed surface with a similar TEM cross section and diffraction analysis as depicted in the "Supporting Information" document (Figs. S8 and S9). We observed the same qualitative and quantitative tendency of the ZnO film growth as for the nickel bottom layer. For the process without the presence of oxygen gas pulsing (Fig. S8), a ZnO film thickness of 1.26 μm was obtained for a growth rate of 2.52 Å/cycle and a film roughness of 190 nm, with sharp grains. We still observed a widening of grain sizes from 70 nm at the bottom to 200 nm on top. The TEM diffraction pattern in Fig. S8(c) showed relatively strong peaks for the ZnO layer coming from grains without privileged orientation. (002) and (100) ZnO are no longer in a preferential position. For the process in the presence of O_2 gas pulsing (Fig. S9), we observed a regular (002) textured ZnO layer with a regular preferential (002) orientation of columnar grains with a constant diameter of 50 nm from bottom to top. The TEM diffraction pattern in Fig. S9(b) clearly revealed

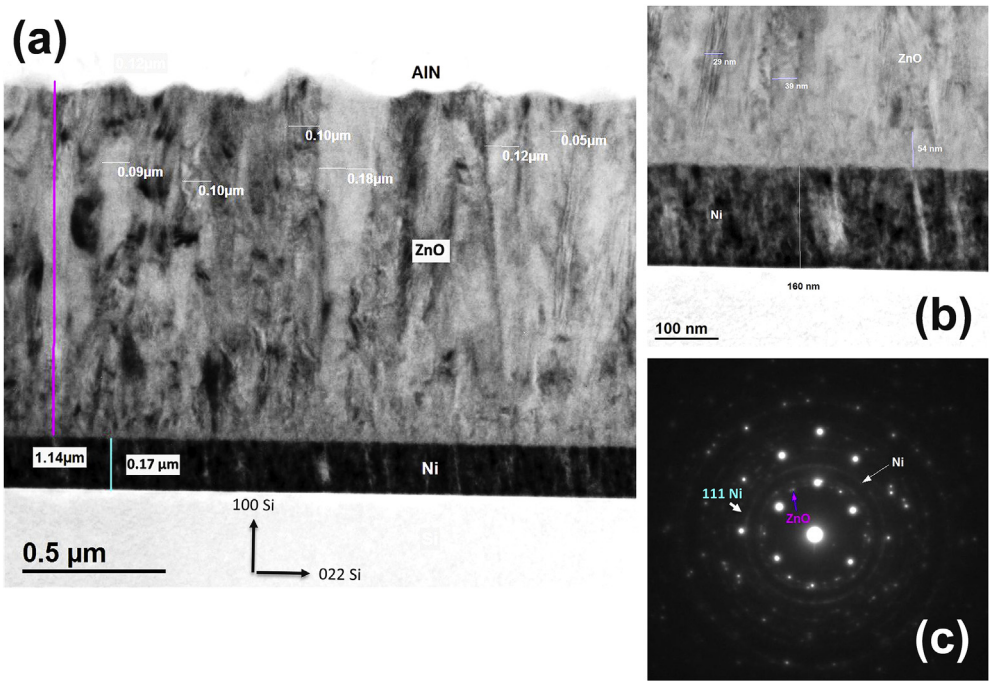

Fig. 4. Transmission Electron Microscopy (TEM) images of ZnO ALD growth during 5000 cycles at a substrate temperature of 180 °C without the presence of O_2 gas pulsing. a) Cross-section view detailing the stacks with nickel as the bottom layer and AlN as the top capping layer. b) Detailed view of the bottom part of the ZnO film at the interface with the nickel layer. c) Diffraction pattern obtained with a 700 nm selected area diaphragm.

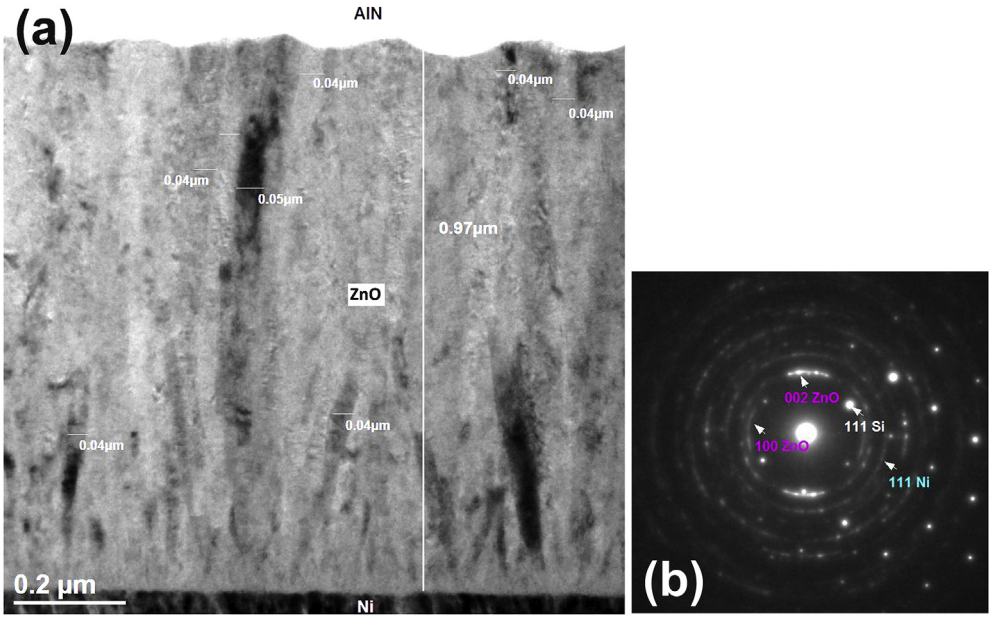

Fig. 5. Transmission Electron Microscopy (TEM) images of ZnO ALD growth during 5000 cycles at a substrate temperature of 180 °C with the presence of O_2 gas pulsing in each cycle. a) Cross-section view detailing the stacks with nickel as the bottom layer and AlN as the top capping layer. b) Diffraction pattern obtained with a 700 nm selected area diaphragm.

an intense peak for ZnO relative to a highly oriented (002).

3.1.2. *Electrical and optical properties*

In order to evaluate the effect of using oxygen gas during ALD growth on the electrical properties of ZnO thin films, we performed four-point probe measurements. Fig. 6 shows the resistivity of ZnO thin films as a function of oxygen pulsing time. There was a huge increase in the resistivity of ZnO thin films when using oxygen gas during ALD synthesis. While the ZnO thin film had a resistivity of about 0.09 Ω cm without using oxygen gas, the ZnO thin films processed with oxygen were around three orders of magnitude more resistive with values of 56.66, 16.77, and 13.72 Ω cm corresponding to ZnO thin films elaborated with 1, 3, and 5 s of O_2 pulses, respectively.

The effects of using oxygen gas during ALD growth on the band gap energy and optical properties of the films can be concluded by measuring the optical transmittance spectrum. Fig. 7 depicts the optical transmittance spectrum of ZnO thin films grown with and without using oxygen gas. The average transmittance of the ZnO films in either the visible

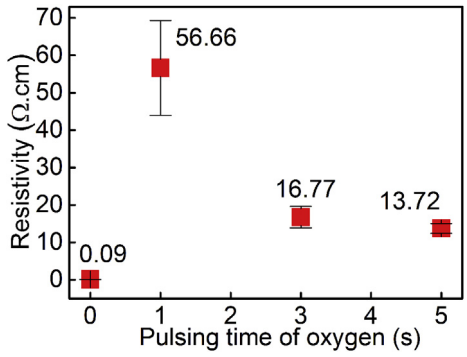

Fig. 6. Resistivity of ZnO thin films as a function of the pulsing time of oxygen gas.

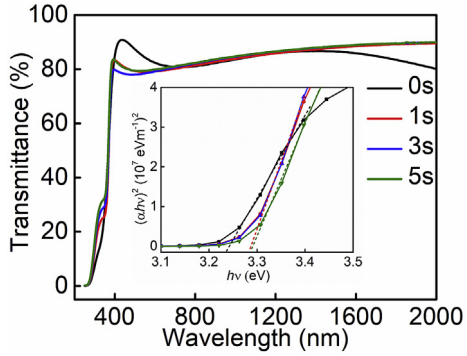

Fig. 7. Optical transmittance spectra of ZnO thin films deposited with different pulsing times of oxygen gas. The inserted figure refers to Tauc plots.

or infrared region was greater than 80% (glass substrate included). The use of oxygen gas during ALD growth induced a higher transmittance of the ZnO films in the infrared domains, whereas a lower transmittance in the visible regions was observed. Namely, the transmittance in infrared and visible regions of ZnO samples with and without oxygen gas is around 85–90% and 80%, 75–80% and 80–92%, respectively. Notably, shallow necks are observed in the UV range (below 400 nm) and their transmittance is higher for the processes with oxygen gas. In fact, these shallow necks were reported before in numerous studies, yet the plausible explanation for it was not mentioned [37–40]. For ZnO nanorods, A. F. Abdulrahman et al. [41] proposed thin films where the transmittance increases when the crystallite size is smaller due to decreased optical scattering. Additionally, the authors mentioned that the transmittance increases with the preferred c-axis orientation, which is consistent with a reduction in light dispersion at grain boundaries as the film structure becomes more oriented along the c-axis. On the other hand, thicker films increase the optical scattering, which reduces the transmittance of the thin layer. Considering the regular (002) textured ZnO was obtained in the presence of oxygen gas during ALD growth, the resulting columnar structure for equivalent film thicknesses and a small grain diameter along the c-axis could fit a similar explanation for the higher transmittance edge in the UV range.

The band-gap energy values of the ZnO thin films can be derived from the Tauc plots, as shown in the detail inserted in Fig. 7. The reflectance and transmittance spectrum of the ZnO films and a reference glass slide was determined to calculate the absorption spectrum of the films (not shown here). For a direct band-gap semiconductor, the relationship between the absorption coefficient α and photon energy $h\nu$ is given by Ref. [42]: $(\alpha h\nu)^2 = A(h\nu - E_g)$. Here, h is Planck's constant; A is a constant and E_g is the optical band gap. By extrapolating the linear part of the Tauc plots to $\alpha = 0$, the band gap can be determined to be about 3.25 eV for the ZnO thin films processed without oxygen gas, and goes up to 3.30 eV for films grown with oxygen pulses, as depicted in Fig. 7. A detailed calculation is given in the Supporting Information.

The room temperature photoluminescence (PL) spectra (Fig. 8) are dominated by strong near band edge (NBE) emission with a peak energy of 3.28–3.31 eV, indicative of the typical excitonic characteristic. The full width at half maximum (FWHM) comprises between 209 and 304 meV for the grown polycrystalline samples, compared with the reference ZnO monocrystalline with a FWHM of 100 meV. The relatively broad linewidth and asymmetric line shape of the NBE emission as compared to the PL signal of the reference single crystal can be attributed to the crystalline quality. For all samples, a broad emission band centered in the green spectral region (2.15–2.35 eV) can also be observed. Although the scientific community has not yet reached a consensus about this visible luminescence, it is accepted that it results from defect-related deep-level emission (DLE), that is, electron transition from the bottom of the conduction band to an antisite defect. The PL intensity ratios of the NBE to DLE emission peaks (I_{NBE}/I_{DLE}) are given in Table 1.

3.1.3. *Compositional and chemical state analyses*

The composition and chemical state of oxygen and zinc have been investigated by x-ray photoelectron spectroscopy (XPS) through analyses of the O 1s and Zn 2p core levels, as illustrated in Fig. 9. The different O/Zn ratios of ZnO thin films are listed in Table 1. It clearly shows that the O/Zn ratios of ZnO thin films deposited using oxygen gas were higher and closer to 1 than that of a ZnO thin film grown without using oxygen gas, corresponding to a lower concentration of oxygen vacancies in the films. It confirms that the higher resistivity achieved in those ZnO thin films is due to fewer oxygen vacancies.

Detailed XPS information of the chemical state of zinc and oxygen was extracted from the Zn 2p and O 1s narrow scans of the ZnO samples. Before any energy calibration, it is worth remarking that the Zn 2p and O 1s peak position of the ZnO film, grown without the presence of oxygen gas, is located at 0.3 eV, a lower binding energy that the ZnO thin films produced with oxygen gas (spectra not shown here). This sample clearly exhibits a lower intrinsic resistivity allowing a better evacuation of the charges. Fig. 7(a) and (b) illustrate the oxidation state of Zn 2p and O 1s core levels and of ZnO thin films, respectively after energy calibration, as well as illustrating intensity normalization for comparison reasons.Whereas the Zn 2p peaks present no evolution according to synthesis conditions, an increase of the shoulder located above 532 eV is observed in the O 1s spectrum when oxygen gas is added in the synthesis process. Generally, the O 1s peak can be adjusted by two components as we did on Fig. S12 (Supplementary Information): a main oxygen peak located at ~ 530.60 eV [43–45] attributed to the O–Zn bonds in a hexagonal wurtzite structure, and a secondary oxygen peak at 532.25 eV, usually related to Zn–OH bonds, chemisorbed oxygen [44,45], or both. For longer pulse times of oxygen gas during the growth, the main and secondary oxygen peaks remain unchanged both positions and relative intensities. The relative intensities of the secondary oxygen peak were about 0% and 10%

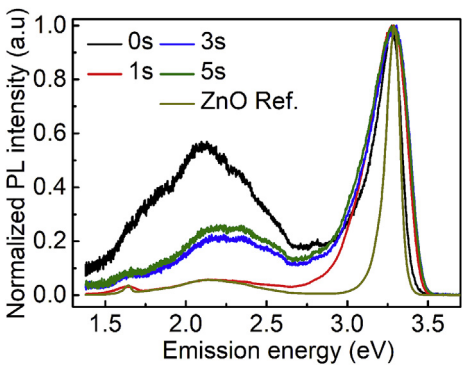

Fig. 8. Photoluminescence spectra of ZnO thin films deposited with different pulsing times of oxygen gas at a constant ALD growth temperature of 180 °C.

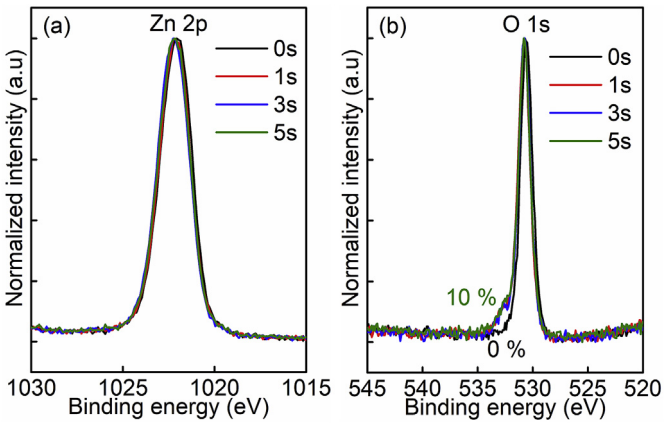

Fig. 9. XPS spectra for ZnO thin films synthesized with different oxygen pulsing times: (a) Zn $2p_{3/2}$ band, (b) O 1s band. The XPS spectra were acquired after Ar + sputter cleaning.

for ZnO films grown without and with oxygen gas, respectively. The binding energy of the secondary oxygen peak can be attributed to Zn–OH bonds originating from water, and/or chemisorbed oxygen. In the case of growing ZnO thin films with oxygen gas, oxygen molecules or ions are adsorbed at grain boundaries [44]. As a result, one possible scenario is a contribution of chemisorbed oxygen on the secondary oxygen peak for the ZnO films using oxygen gas during growth. This scenario will be elaborated further in the Discussion section. It is worth mentioning that an increase in the full-width-half-maximum of the O 1s peak in association with the shift of Zn 2p peak could confirm the presence of oxygen vacancies, leading to a low resistivity of the ZnO films fabricated without oxygen gas.

3.2. Effect of substrate temperature

3.2.1. Crystallographic structure and morphologic properties

Fig. 10(a) shows the growth rate of ZnO thin films grown with 1-s oxygen gas pulsing at different substrate temperatures. It can be seen that the growth rate increased monotonously with substrate temperatures from 100 °C to 200 °C. This result differs from previous reports on the dependence of the growth rate on substrate temperatures for ZnO thin film grown with DEZ and DI water as precursors [46,47]. In those studies, it was shown that the growth rate of ZnO thin films was almost unchanged for temperatures ranging from 100 °C to 180 °C, which is the so-called ALD growth window. The growth window describes a temperature range where the growth rate is both constant and self-limited due to the balance between chemical reactivity and physical desorption. Interestingly, the growth rate of ZnO thin films in our experiment did not follow these studies, but increased constantly in the investigated temperature range of 100–200 °C. This implies that, by inserting the oxygen gas during ALD processes, the equilibrium between chemical reactivity and physical desorption in our experiment could be broken and the growth window in this case could be shifted to a higher temperature range.

The evolution of the crystallographic structure of ZnO thin films was evaluated by GIXRD, as shown in Fig. 10(b). It clearly shows the dominance of the (002) diffraction peak of the ZnO thin films at above 150 °C. Particularly, the ZnO thin films possess highly oriented (002) crystal orientation at 180 °C and 200 °C, indicating film growth with the c-axis perpendicular to the substrate surface. At the low temperature of 100 °C, however, the preferred (002) orientation is lost, and the diffraction pattern displays a contribution of non-polar (100) and (101) planes, as well as polar planes (002). This is consistent with previous reports [27,28], which showed that (100) and (002) diffraction peaks were found for ZnO thin films deposited at low substrate temperatures (135–150 °C). The degradation of the (002) preferred orientation can be caused by the suppression of crystal growth in this temperature range. As shown in Table 1, the GI-TC was calculated to quantify the preferred orientations of the films. According to the GI-TC calculation, a highly preferred (002) orientation was observed on the films grown at 180 °C and 200 °C, i.e. GI-TC (002) > 2.5 for the three Bragg reflections considered. The films grown at 150 °C and especially at 100 °C show a more isotropic randomly oriented distribution of (100), (002) and (101) crystallographic orientations, i.e. GI-TC (002) < 2.5 for the three Bragg reflections considered (see Fig. S4, Supporting Information).

It is also worth mentioning that the shift of the (002) peak can be observed on ZnO thin films grown under oxygen gas with different substrate temperatures, as listed in Table 1. The (002) peak shifted to higher angles with increasing substrate temperatures, as illustrated in Fig. 10(b). For example, it was 34.28° and 34.50° for the ZnO thin films processed at 100 °C and 200 °C. Notably, the (002) peak of the ZnO films at 200 °C is likely to return to the (002) peak position of the ZnO films grown at 180 °C without using oxygen gas. This could imply that the oxygen gas desorption on the film surface or a change in the chemisorption processes (from molecular to ionic form) could occur at 200 °C [48].

SEM micrographs (Fig. 11) strongly confirmed the evolution of a crystallographic structure displayed on XRD data. While at high temperatures, the ZnO thin films contains fine-columnar grains perpendicular to the substrate surface, the ZnO thin films grown at lower temperatures display a distribution of grains with their polar c-axis perpendicular and parallel to the substrate surface (Fig. S7, Supporting Information). It was also found that the crystalline distribution of ZnO thin film elaborated at 100 °C with an oxygen gas pulsing (Fig. S10,

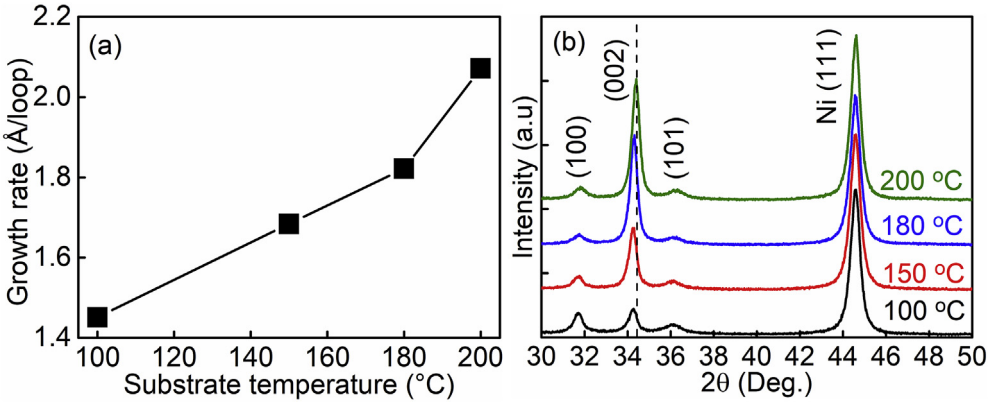

Fig. 10. (a) Growth rate, and (b) grazing incidence x-ray diffraction pattern ($\omega = 0.5°$) of ZnO thin films with different growing temperatures. The nickel (111) peak was used as a reference to track the shift of the diffraction peaks of ZnO films. The black dashed vertical line highlights the shift of the (002) peak.

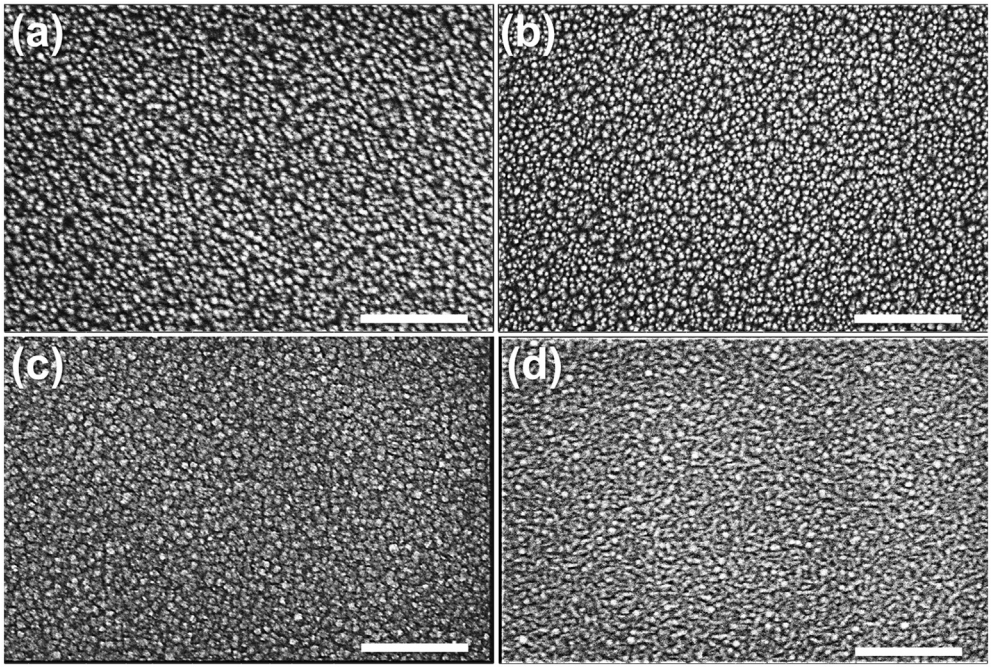

Fig. 11. SEM top-view micrographs of ZnO thin films with different substrate temperatures (a) 200 °C, (b) 180 °C, (c) 150 °C, and (d) 100 °C. The scale bar is 300 nm.

Supporting Information) is very similar to that of a ZnO thin film synthesized without oxygen gas at 180 °C (Fig. 2(a)), but the grain size is slightly finer from 6 to 16 nm average diameters.

3.2.2. *Electrical and optical properties*

Fig. 12 illustrates a substrate temperature resistivity dependence of ZnO thin films grown in the presence of oxygen gas. In general, the resistivity decreases as the substrate temperature increases. With the exception of the film grown at 180 °C, the resistivity was a bit higher than that of the film at 150 °C. There were about 1196.08, 45.02, 56.66, and 14.39 Ω cm for the ZnO thin films grown at 100, 150, 180 and 200 °C. It should be noted that the resistivity of the ZnO thin film grown at 100 °C was significantly higher than that of others and four orders of magnitude higher than that of the ZnO thin film grown at 180 °C without oxygen. This increase of resistivity at low processing temperatures has been reported previously [48,49]. The plausible reason for this is a lower carrier concentration at lower substrate temperatures in which the resistivity is mainly determined by inter-grain (grain boundary) transport [50,51]. The inter-grain scattering is due to the build-up of potential barriers from the trapping of electrons at the grain boundaries. To confirm the correlation, Hall measurements were performed in the van der Pauw configuration to determine the carrier concentration of the ZnO thin films without and with using oxygen gas. The carrier concentration was 7.11 $\times$ 10^{19} cm^{-3} and 4.08 $\times$ 10^{16} cm^{-3} for the ZnO thin films grown at 180 °C without and with oxygen with a pulsing time of 1 s, respectively. The carrier concentration of the ZnO thin film grown at 100 °C with oxygen gas pulsing was estimated at 10^{14} cm^{-3} due to the limit of the Hall measurement with our equipment for highly insulating materials, as reported by F. Werner for low mobility polycrystalline thin films [52]. In addition, in our processes, chemisorbed oxygen molecules can be trapped at the grain boundaries, which will increase the potential barrier, preventing inter-grain electrical transport. Therefore, in this study, a simultaneous contribution of two phenomena will further decrease the electrical conductivity of ZnO thin films.

Optical transmittance spectroscopy was carried out to study the impact of substrate temperatures on the optical properties of ZnO thin films (Fig. 13). The average transmittance values of all thin films were above 80% in the visible and infrared regions except for the film grown at 100 °C. It should be pointed out that the transmittance values in the visible region slightly increased as substrate temperatures went up. The Tauc plots were also performed to determine the optical band gap of those films, as displayed in the insert in Fig. 13. The band gap values of the ZnO films grown at 150 °C and above are all equal to 3.29 eV while that of the film grown at 100 °C was slightly larger with 3.33 eV, as depicted in Fig. S13 (Supporting Information).

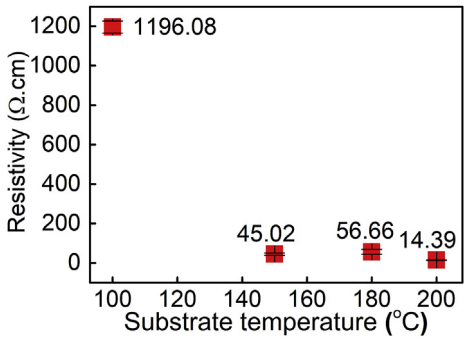

Fig. 12. Resistivity of ZnO thin films deposited at different substrate temperatures.

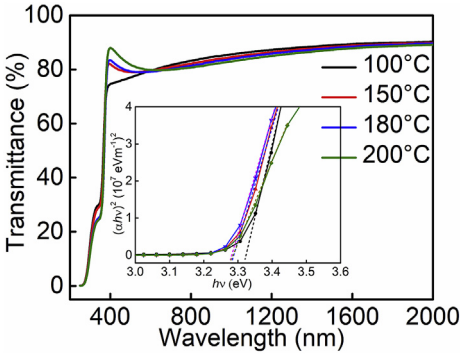

Fig. 13. Optical transmittance spectroscopy of ZnO thin films deposited at different substrate temperatures. The inserted figure refers to Tauc plots.

Here also, the room temperature PL spectra (Fig. 14) are dominated by strong excitonic NBE emissions with peak energy between 3.26 and 3.31 eV. The FWHM of the NBE emission peaks comprises between 278 and 368 meV for the grown polycrystalline samples, compared with the reference ZnO monocrystalline with a FWHM of 100 meV. The broad-band emission band centered in the green spectral region (2.15–2.35 eV) can also be observed for every sample. The PL intensity ratios of the NBE to DLE emission peaks (I_{NBE}/I_{DLE}) are indicated in Table 1.

3.2.3. Compositional and chemical state analysis

X-ray photoelectron spectroscopy was carried out to study the influence of substrate temperatures on the chemical stoichiometry and surface bonding of the ZnO films. The in-depth O/Zn ratio was used to understand the effect of substrate temperature on the stoichiometry of the ZnO films. It is clearly shown in Table 1 that the highest value of O/Zn ratio belonged to the film grown at a low temperature of 100 °C, whereas the values of the films grown above 150 °C remain almost unchanged. This is consistent with the discussion by E. Guziewicz et al., and T. S. Bjørheim et al. [47,53] that the formation of defects, such as zinc or oxygen vacancies, can be suppressed in the low temperature regime because of insufficient activation energy.

Binding energies of Zn 2p and O 1s bands are presented in Fig. 15(a)-(b), respectively. The shape of both peaks is very similar. No deviation of the binding energies can be observed on Zn 2p and O 1s bands of the ZnO thin films grown at different substrate temperatures. As noted in Fig. 15(b), the O 1s peak can also be fitted with two sub-peaks, i.e. a main peak at around 530.60 eV indicates the Zn–O bonding in the wurtzite structure, and a secondary peak (532.25 eV) attributed to Zn–OH bonding and/or chemisorbed oxygen.

4. Discussion

4.1. Correlations of chemical composition, optical properties, and electrical properties

It has been pointed out that the electronic trapping at grain boundaries plays an important role in the electrical properties of polycrystalline semiconductors [53–56]. The local charge of these traps induces a potential build-up barrier for the electrons, which impedes the current flow through the grain boundary [54]. In the presence of oxygen gas, oxygen will be chemisorbed in form of molecular O_2^- and/or atomic (O^-, O^{2-}) ions [48] and will be trapped at the grain boundary [46]. Here, absorbed oxygen species can capture electrons from the surface and inner of grains, and then create depletion regions, which further increase the potential barriers at the grain boundaries. Consequently, the potential barriers prevent the electron flow, leading to an increase in resistivity of the ZnO films. This was the situation for the ZnO thin films grown with oxygen gas.

In general, the free charge carriers of intrinsic ZnO are mainly related to some native defects, such as oxygen vacancies, which acts as donors, increasing the surface conductivity. In an oxygen-rich environment, the relatively large amount of chemisorbed oxygen species, acting as surface acceptors, will neutralize the oxygen vacancies and donors, thus reduce the surface conductivity [48]. The chemical composition and appearances of the secondary oxygen peaks (532.25 eV) in XPS have confirmed the suitable stoichiometry promoting the presence of oxygen on zinc in ZnO thin films grown in the presence of oxygen gas. A stoichiometric ratio O/Zn that is closer to one makes a film of higher resistivity. In fact, the highest resistivity of our films (1196.08 Ω cm) was achieved on the ZnO films grown at 100 °C with the highest value of O/Zn ratio (0.98). A possible reason for interpreting the increase in resistivity of the ZnO thin films can be based on chemisorption processes of oxygen gas on the semiconducting surface. For the ALD processes with oxygen gas, oxygen molecules are adsorbed on the surface of the ZnO thin films [48,57]. Those oxygen molecules absorbed play as scavengers, which can capture electrons from the surface and the interior of the ZnO film [58,59]. The

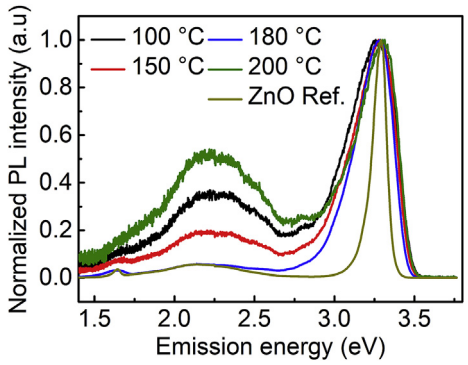

Fig. 14. Photoluminescence spectra of ZnO thin films deposited at different substrate temperatures at a constant O_2 pulse time of 1 s during ALD growth. The spectra have been normalized for the sake of clarity.

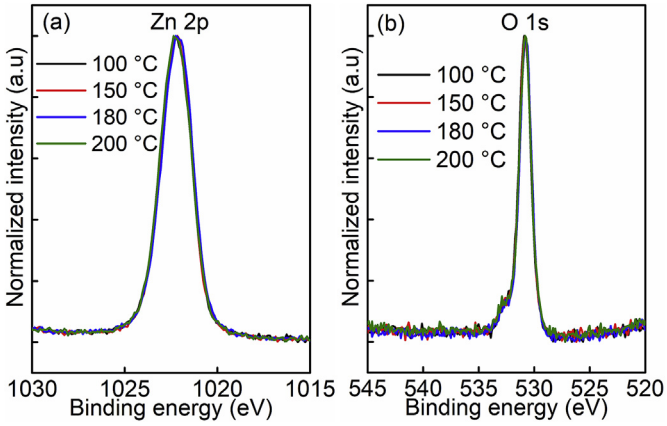

Fig. 15. XPS spectra for ZnO thin films synthesized at different substrate temperatures: (a) Zn $2p_{3/2}$ band, (b) O 1s band. The XPS spectra were acquired after Ar + sputter cleaning. The XPS spectra for ZnO thin films synthesized at different substrate temperatures: (a) Zn $2p_{3/2}$ band, (b) O 1s band.

electron trapped in oxygen species causes a depletion layer, leading to an increase in resistivity [48,57]. Depending on working temperatures, adsorbed oxygen can appear in the form of molecular O_2^- and/or atomic (O^-, O^{2-}) ions. In general, this is controlled by the working temperature: below 150 °C, the molecular form dominates while atomic ions dominate above 150 °C. In our case, with ZnO thin films grown at 180 °C, the presence of atomic ions would dominate.

In addition, the visible region of the photoluminescence spectra illustrated the presence of deep-level emission (DLE) defects against the ALD process parameters: the presence of the O_2 pulses in the sequence and the sample temperature during growth. These DLE defects come from impurities or defects with high ionization energy located deep in the band gap. It is accepted that these deep levels are mainly due to intrinsic defects, impurities and/or a combination of both. Although their nature remains uncertain with often contradictory explanations, there are three main commonly accepted emission regions [60–62]:

(i) The green domain (G1) is located in a wavelength range of ~480–550 nm (~2.58–2.25 eV). This emission has been associated with gaps in oxygen vacancies simply ionized (V_O°), or oxygen antisites, or even zinc vacancies (V_{Zn}°).
(ii) The yellow-orange emission (G2) has wavelengths of ~550–610 nm (~2.25–2.03 eV). This corresponds to the gaps of oxygen vacancies doubly ionized (VO°), and interstitial oxygen (Oi).
(iii) The red emission (G3) of ~610–755 nm (~2.03–1.64 eV) has been attributed to excess oxygen on the ZnO surface.

As a result, it can be observed that the ALD processed at 180 °C with 1 s of oxygen gas pulsing has a larger intensity ratio of NBE to DLE emission peaks (I_{NBE}/I_{DLE}) (Table 1) with a defect presence comparable to the reference ZnO single crystal. It can also be noted that the PL spectra (Fig. 8) in the visible region (2.0–2.5 eV) shows a similar trend in electrical resistivity (Fig. 6) to ZnO thin films grown at 180 °C and with 1–5 s of oxygen pulse time. The 1s pulse sample presents the highest resistivity and the lowest relative visible photoluminescence emissions compared to the other pulse duration samples. The XPS analysis performed on the samples rules out the hypothesis of the presence of a significant amount of impurities (Fig. S11, Supporting Information). As a general tendency, the presence of O_2 during the processes allowed the intensity ratio of the NBE to DLE emission peak to be increased probably by reducing the oxygen vacancy defects. This opens an interesting perspective to improve the UV light emission efficiency of ZnO in LED devices, with the possibility of simultaneously modulating the electrical resistivity of the material.

The dependence of electrical properties on the surface morphology has been discussed previously in several works [27,48,49]. A higher carrier concentration was found in the polar-plane (002)-texture films, whereas a lower carrier concentration was displayed in the non-polar (100), (101)-texture films. Furthermore, the higher carrier concentration was in concomitant with the higher defect density or lower stoichiometry of the ZnO films. It is consistent with our observation, even though the polar-plane (002) films grown with oxygen shown higher resistivity in contrast to the ZnO films grown without oxygen. On the other hand, a too large amount of oxygen during the ALD process with pulsing times of 3 s and 5 s induced a decrease in resistivity (see Fig. 6), but with a similar optical band gap as for 1 s of oxygen pulse grown samples. The corresponding PL spectra (Fig. 8) showed an increase of the yellow-orange emission (G2), which is a possible signature of interstitial oxygen. The picture is different in the most resistive ZnO films grown with oxygen at 100 °C, which show random crystallographic orientations, but the chemical composition was found to be the most stoichiometric in comparison to other films.

Moreover, TEM analysis in cross-section and diffraction patterns illustrates the similar growth profiles of ZnO films (rough polycrystalline with grains widening and regular (002) texture with columnar grains, with and without the presence of the oxygen gas pulsing respectively) on either a metallic (nickel) or an insulating (AlN) bottom seed layers. This implies that the buffer layers have no significant impact on the ZnO thin film structuring during growth. In addition, the detailed cross section by TEM shows that the grains are actually interconnected at their bases.

A remarkable correlation between the chemical composition and the optical band gap is observed. The optical band gap increased when the O/Zn ratio increased in the ZnO films grown with oxygen gas. This can be understood as a filling of oxygen vacancies, annihilating the shadow donor levels [27,59,63]. Interestingly, we noticed an evolution of the strain to band gap energy as observed by T. Singh et al. [64] with an increase of the band gap level against an increase of the tensile strain in the ZnO thin film (Fig. S13, Supporting Information). The authors correlated the ZnO film thickness with the induced inner strain. Table 1 relates the net out-of-plane strain calculated from changes of the c lattice parameter. According to the strain-to-thickness relationship measured by T. Singh et al. [64], in Table 1 we indicated the relative change of the strain in absolute value due to the modulation of the thicknesses being lower than that calculated from the c lattice parameter change measured by GIXRD. This indicates a substantial contribution of the crystalline orientation and/or chemical composition and relative impurities and defects of the film compared to the thickness parameter on the induced strain relative to the different ALD processes.

4.2. Growth mechanisms of (002) preferred orientation

Control of the preferred orientation of ZnO thin films has been investigated here with two varying thermodynamic parameters during the growth. Among deposition parameters such as the pulsing time of precursors [65] and the substrate temperature, the temperature during deposition was the most commonly used, as it enables the crystallographic orientation of the ZnO film to be controlled in a very efficient way [27,28]. Three zones were identified based on the predominance of (100) and (002) orientations: zone 1 (135–155 °C) where the films are dominated by (100) and (002)-oriented crystallites; zone 2 (155–220 °C) with a dominant (100) orientation and finally zone 3 at higher temperatures (220–300 °C) where the (002) orientation dominates. This suppression of the (002) crystallographic orientation in the temperature range of 155–220 °C has been discussed in previous works [27,28]. It could be better understood by considering stacking sequences of the ZnO (002) polar-plane, which can be seen as Zn/O/Zn/O … stacking sequences of the hexagonal type AbBaA … along its polar c-axis [66]. As a result, the (002) polar surface could be negatively or positively charged, corresponding to oxygen ion terminated ZnO $(00\bar{1})$-O or zinc ion terminated ZnO (0001)-Zn. In the temperature range of 150–300 °C, it has been demonstrated that the premature dissociation of DEZ precursors may occur [67–69]. The dissociated ethyl groups can be cleaved further into ethyl and methyl group fragments, such as CH_3CH_2 and CH_3 in the temperature range of 150–220 °C [28]. These anions can bond to the positively charged ZnO (0001)-Zn polar surface, which prevents growth along the polar c-axis direction. Our ZnO thin films, grown without using oxygen gas during ALD processes, follows this abovementioned argument. In fact, the films show a crystallographic contribution of the nonpolar-plane (100), (101) and polar-plane (002) orientations. However, this was no longer the case for the ZnO thin films processed in an oxygen-rich environment, where the (002) polar-plane orientation became a preferred orientation. It can be interpreted by a picture of cleave/combustion processes during ALD growth. M. A. Thomas et al. [30] pointed out that energetic O radicals from oxygen plasma cleave/-combust the ligands CH_3CH_2 and CH_3, which are bonded to Zn and subsequently oxidize Zn. In our situation, when absorbing molecular oxygen on the polar surface, the charges from the ZnO surface transferred to the antibonding π^* orbitals of oxygen, transforming it into a peroxo radical (O_2^{-2}) [58]. This can act as a reactive oxidant and homolytic fission agent. Therefore, the surface in an oxygen-rich environment can be cleaned up by further removing the ligands of ethyl groups. Consequently, the (002)-oriented growth direction will be no longer suppressed, but will keep growing and dominating with its lowest surface energy for the fastest growth rate [25].

The growth mechanism of (002) the polar-plane orientation could also be pinpointed by reviewing a stabilization aspect of the polar surface, which has received significant considerations in the last few decades [70–73]. Generally, the most crucial point of the growing (002) texture is to control the formation of tetrahedral coordination sp^3 in the vapor phase and at the substrate surface in order to change the equilibrium state of the deposition [25]. Fujimura et al. [25] demonstrated that a suitable sputtering gas condition with the ratio $Ar:O_2 = 4:1$ promoted the tetrahedral coordination in the vapor phase. The suitable gas condition could be related to the polar surface stabilization. In fact, on the polar surface of sp^3 hybridized tetrahedral coordination, the fulfilment of electron counting has to satisfy a local charge-neutral surface and the vanishment of the macroscopic dipole, by electrostatically stabilizing the surface [73–75]. Several possible methods for this have been proposed, i.e. the formation of 0.25 ml (monolayer) of zinc vacancies; adsorption of 0.25 ml O_2 or combinations thereof for the case of ZnO (0001)-Zn polar surface. Correspondingly, the ZnO $(00\bar{1})$-O polar termination can be electrostatically stabilized through oxygen deficiency. P. Gorai et al. revealed that theoretically, the lowest adsorption enthalpies were found on the ZnO (0001)–Zn polar surface reconstruction that were formed under O-rich and H-poor environments and stabilized by adsorbing O species [58]. By contrast, ZnO $(00\bar{1})$–O surfaces were found to be stabilized by involving adsorbed H under O-rich conditions. In our studies, the preferred (002) oriented films were synthesized in an oxygen-rich environment. Therefore, the ZnO (0001)–Zn polar surface

reconstruction could be the most stable surface by adsorbing oxygen adatoms and/or oxygen molecules; this was confirmed by the appearance of the secondary oxygen peak in XPS spectra. In the same time, the (002) surface possesses the lowest surface energies (0.099 eV/Å^2) in comparison to (100) and (101) surfaces, which are 0.123 and 0.209 eV/Å^2, respectively. As a result, the (002)-oriented ZnO film keeps growing in the preferable way.

5. Conclusion

In summary, the crystallographic, morphological, electrical, optical, and electronic properties have been explored and evaluated for zinc oxide thin films elaborated by thermal atomic layer deposition in the presence of O_2 pulses in the process. It has been demonstrated that using oxygen gas during atomic layer deposition could profoundly affect the properties of zinc oxide thin films. The crystalline structure can be highly tuned from nonpolar plane orientations to a polar plane orientation by inserting oxygen gas. The electrical resistivity of the films grown under O_2 conditions shown a dramatic increase of 3–4 orders of magnitude contrary to that of the film grown without oxygen gas. It could be interesting for improving the issue of current leakage for piezoelectric applications of thin film ZnO as actuators or strain sensors. On the other hand, the electrical properties and optical properties strongly correlated to the electronic properties and chemical composition of zinc oxide thin film. Indeed, the highest resistivity and the largest band gap were found on the zinc oxide deposited with oxygen gas at the substrate temperature of 100 °C, due to it having the lowest oxygen deficiency in comparison with other samples. The intensity ratio of the near band edge emission to the deep-level emission peak, with the deep-level emission caused by defects located deep in the band gap, can be increased by applying an adequate pulsing of oxygen gas during the process. This would have a positive impact on the UV light emission efficiency of ZnO devices such as LED. Also, several hypotheses were discussed in order to understand the dominance of (002) orientation in the presence of oxygen during atomic layer deposition; (i) homolytic fission of residual organic ligands by peroxo radical (O_2^{-2}), (ii) reconstruction and stabilization of the polar surfaces. It could be possible that both mechanisms contribute simultaneously to the growth of a film with a (002) preferred orientation. This theory should be tested by means of a theoretical calculation or molecular dynamic simulation in order to have a complete picture of growth mechanism. However, our study provides reliable methods to tailor the preferred orientations and the optical and electrical properties of the zinc oxide thin films in a simple and inexpensive way that is compatible with the semiconductor industry in order to provide a possible benefit to related applications.

Data availability

The raw/processed data required to reproduce these findings cannot be shared at this time due to technical or time limitations.

Authorship contribution statement

The manuscript was written with contributions from all authors. All authors have given their approval to the final version of the manuscript.

Declaration of competing interest

The authors declare that there are no competing interests.

The authors declare that they have no known competing financial interests or personal relationships that could have appeared to influence the work reported in this paper.

Credit authorship contribution statement

Tai Nguyen: Methodology, experiments (ALD processes, characterizations), manuscript writing - original draft. **Noureddine Adjeroud**: Methodology, experiments (ALD processes). **Mael Guennou**: Photoluminescence analysis and data interpretation, review & editing. **Jérôme Guillot**: XPS analysis and data interpretation, review & editing. **Yves Fleming**: XRD and pole figure analysis and data interpretation, review & editing. **Anne-Marie Papon**: TEM cross section and diffraction analysis and data interpretation, review & editing. **Didier Arl**: SEM analysis and data interpretation, review & editing. **Kevin Menguelti**: experiments (ALD processes, samples preparation). **Raoul Joly**: experiments (ALD processes), review & editing. **Narciso Gambacorti**: TEM data interpretation. **Jérôme Polesel Maris**: Project manager, supervisor, ALD experiments, data analysis, funding acquisition, manuscript writing, review & editing.

Declaration of competing interest

The authors declare that there are no competing interests.

The authors declare that they have no known competing financial interests or personal relationships that could have appeared to influence the work reported in this paper.

Acknowledgements

The authors acknowledge Dr. Petru Lunca Popa for support on optical spectra measurements, Dr. Inmaculada Peral Alonso for facilitating the NFFA collaboration, and Dr. Naoufal Bahlawane for fruitful discussions and advice. The authors gratefully acknowledge the financial assistance provided by the FNR in the framework of the FNR CORE project PSSENS (Project ref.: PSSENS C16/MS/11349047) and the FNR PRIDE MASSENA 15/10935404/MASSENA for funding. The authors acknowledge the contribution of the Nanoscience Foundries and Fine Analysis (NFFA) European Research Infrastructure. In fact, this project has received funding from the EU-H2020 research and innovation program under grant agreement No 654360, and benefitted from the access provided by Laboratoire d'électronique des technologies de l'information (CEA-LETI) in Grenoble.

Appendix A. Supplementary data

Supplementary data to this article can be found online at https://doi.org/10.1016/j.rinma.2020.100088.

References

[1] Ü. Özgür, Y.I. Alivov, C. Liu, A. Teke, M.A. Reshchikov, S. Doğan, V. Avrutin, S.J. Cho, H. Morkoç, A comprehensive review of ZnO materials and devices, J. Appl. Phys. 98 (2005), 041301, https://doi.org/10.1063/1.1992666.

[2] B.J. Jin, S.H. Bae, S.Y. Lee, S. Im, Effects of native defects on optical and electrical properties of ZnO prepared by pulsed laser deposition, Mater. Sci. Eng. B Solid-State Mater. Adv. Technol. 71 (2000) 301–305, https://doi.org/10.1016/S0921-5107(99)00395-5.

[3] R.F. Service, Will UV lasers beat the blues? Science 276 (1997) https://doi.org/10.1126/science.276.5314.895, 895-895.

[4] Y. Yuan, K. Shyong Chow, H. Du, P. Wang, M. Zhang, S. Yu, B. Liu, A ZnO thin-film driven microcantilever for nanoscale actuation and sensing, Int. J. Smart Nano Mater. 4 (2013) 128–141, https://doi.org/10.1080/19475411.2012.749959.

[5] Y.S. Choi, J.W. Kang, D.K. Hwang, S.J. Park, Recent advances in ZnO-based light-emitting diodes, IEEE Trans. Electron. Dev. 57 (2010) 26–41, https://doi.org/10.1109/TED.2009.2033769.

[6] P.K. Nayak, J. Yang, J. Kim, S. Chung, J. Jeong, C. Lee, Y. Hong, Spin-coated Ga-doped ZnO transparent conducting thin films for organic light-emitting diodes, J. Phys. D Appl. Phys. 42 (2009), 035102, https://doi.org/10.1088/0022-3727/42/3/035102.

[7] R.S. Mane, W.J. Lee, H.M. Pathan, S.H. Han, Nanocrystalline TiO_2/ZnO thin films: fabrication and application to dye-sensitized solar cells, J. Phys. Chem. B 109 (2005) 24254–24259, https://doi.org/10.1021/jp0531560.

[8] T. Van Dang, N. Duc Hoa, N. Van Duy, N. Van Hieu, Chlorine gas sensing performance of on-chip grown ZnO, WO_3, and SnO_2 nanowire sensors, ACS Appl. Mater. Interfaces 8 (2016) 4828–4837, https://doi.org/10.1021/acsami.5b08638.

[9] N.D. Khoang, D.D. Trung, N. Van Duy, N.D. Hoa, N. Van Hieu, Design of SnO_2/ZnO hierarchical nanostructures for enhanced ethanol gas-sensing performance, Sensor.

Actuator. B Chem. 174 (2012) 594–601, https://doi.org/10.1016/j.snb.2012.07.118.
[10] L. Le Brizoual, F. Sarry, O. Elmazria, P. Alnot, S. Ballandras, T. Pastureaud, GHz frequency ZnO/Si SAW device, IEEE Trans. Ultrason. Ferroelectrics Freq. Contr. 55 (2008) 442–450, https://doi.org/10.1109/TUFFC.2008.662.
[11] Z.L. Wang, X. Wang, J. Song, J. Liu, Y. Gao, Piezoelectric nanogenerators for self-powered nanodevices, IEEE Pervasive Comput 7 (2008) 49–55, https://doi.org/10.1109/MPRV.2008.14.
[12] Z.L. Wang, J. Song, Piezoelectric nanogenerators based on zinc oxide nanowire arrays, Science 312 (2006) 242–246, https://doi.org/10.1126/science.1124005.
[13] J. Briscoe, S. Dunn, Piezoelectric nanogenerators - a review of nanostructured piezoelectric energy harvesters, Nanomater. Energy 14 (2014) 15–29, https://doi.org/10.1016/j.nanoen.2014.11.059.
[14] R. Hinchet, S. Lee, G. Ardila, L. Montès, M. Mouis, Z.L. Wang, Performance optimization of vertical nanowire-based piezoelectric nanogenerators, Adv. Funct. Mater. 24 (2014) 971–977, https://doi.org/10.1002/adfm.201302157.
[15] Y. Liu, Y. Li, H. Zeng, ZnO-based transparent conductive thin films: doping, performance, and processing, J. Nanomater. 2013 (2013) 196521, https://doi.org/10.1155/2013/196521.
[16] T. Wang, H. Wu, H. Zheng, J.B. Wang, Z. Wang, C. Chen, Y. Xu, C. Liu, Nonpolar light emitting diodes of m-plane ZnO on c-plane GaN with the Al_2O_3 interlayer, Appl. Phys. Lett. 102 (2013) 141912, https://doi.org/10.1063/1.4801761.
[17] K.J. Loh, D. Chang, Zinc oxide nanoparticle-polymeric thin films for dynamic strain sensing, J. Mater. Sci. 46 (2011) 228–237, https://doi.org/10.1007/s10853-010-4940-3.
[18] W. Wu, Z.L. Wang, Piezotronics and piezo-phototronics for adaptive electronics and optoelectronics, Nat. Rev. Mater. 1 (2016) 16031, https://doi.org/10.1038/natrevmats.2016.31.
[19] Z.L. Wang, Piezopotential gated nanowire devices: piezotronics and piezo-phototronics, Nano Today 5 (2010) 540–555, https://doi.org/10.1016/j.nantod.2010.10.008.
[20] Z.L. Wang, W. Wu, Piezotronics and piezo-phototronics: fundamentals and applications, Natl. Sci. Rev. 1 (2014) 62–90, https://doi.org/10.1093/nsr/nwt002.
[21] Z.L. Wang, Progress in piezotronics and piezo-phototronics, Adv. Mater. 24 (2012) 4632–4646, https://doi.org/10.1016/j.scitotenv.2007.05.034.
[22] Z.L. Wang, X. Wang, Nanogenerators and piezotronics, Nanomater. Energy 14 (2015) 1–2, https://doi.org/10.1016/j.nanoen.2015.01.011.
[23] P. Wang, H. Du, ZnO thin film piezoelectric MEMS vibration energy harvesters with two piezoelectric elements for higher output performance, Rev. Sci. Instrum. 86 (2015), 075002, https://doi.org/10.1063/1.4923456.
[24] M. Miura, Crystallographic character of ZnO thin film formed at low sputtering gas pressure, Jpn. J. Appl. Phys. 21 (1982) 264–272, https://doi.org/10.1143/JJAP.21.264.
[25] N. Fujimura, T. Nishihara, S. Goto, J. Xu, T. Ito, Control of preferred orientation for ZnOx films: control of self-texture, J. Cryst. Growth 130 (1993) 269–279, https://doi.org/10.1016/0022-0248(93)90861-P.
[26] F.K. Shan, B.C. Shin, S.W. Jang, Y.S. Yu, Substrate effects of ZnO thin films prepared by PLD technique, J. Eur. Ceram. Soc. 24 (2004) 1015–1018, https://doi.org/10.1016/S0955-2219(03)00397-2.
[27] C.H. Chao, P.W. Chi, D.H. Wei, Investigations on the crystallographic orientation induced surface morphology evolution of ZnO thin films and their wettability and conductivity, J. Phys. Chem. C 120 (2016) 8210–8219, https://doi.org/10.1021/acs.jpcc.6b01573.
[28] S.Y. Pung, K.L. Choy, X. Hou, C. Shan, Preferential growth of ZnO thin films by the atomic layer deposition technique, Nanotechnology 19 (2008) 435609, https://doi.org/10.1088/0957-4484/19/43/435609.
[29] T.A. Krajewski, K. Dybko, G. Luka, E. Guziewicz, P. Nowakowski, B.S. Witkowski, R. Jakiela, L. Wachnicki, A. Kaminska, A. Suchocki, M. Godlewski, Dominant shallow donors in zinc oxide layers obtained by low-temperature atomic layer deposition: electrical and optical investigations, Acta Mater. 65 (2014) 69–75, https://doi.org/10.1016/j.actamat.2013.11.054.
[30] M.A. Thomas, J.B. Cui, Highly tunable electrical properties in undoped ZnO grown by plasma enhanced thermal-atomic layer deposition, ACS Appl. Mater. Interfaces 4 (2012) 3122–3128, https://doi.org/10.1021/am300458q.
[31] R. Huang, S. Ye, K. Sun, K.S. Kiang, C.H.K. de Groot, Fermi level tuning of ZnO films through supercycled atomic layer deposition, Nanoscale Res. Lett. 12 (2017) 541, https://doi.org/10.1186/s11671-017-2308-1.
[32] S.H.K. Park, Y.E. Lee, Controlling preferred orientation of ZnO thin films by atomic layer deposition, J. Mater. Sci. 39 (2004) 2195–2197, https://doi.org/10.1023/B:JMSC.0000017786.81842.ae.
[33] F. Bachmann, R. Hielscher, H. Schaeben, Texture analysis with MTEX – free and open source software toolbox, Solid State Phenom. 160 (2010) 63–68, 10.4028/www.scientific .net/ssp.160.63.
[34] G.B. Harris, X., Quantitative measurement of preferred orientation in rolled uranium bars, London, Edinburgh, Dublin Philos. Mag. J. Sci. 43 (1952) 113–123, https://doi.org/10.1080/14786440108520972.
[35] H.R. Moutinho, F.S. Hasoon, F. Abulfotuh, L.L. Kazmerski, Investigation of polycrystalline CdTe thin films deposited by physical vapor deposition, close-spaced sublimation, and sputtering, J. Vac. Sci. Technol. A Vacuum, Surfaces, Film. 13 (1995) 2877, https://doi.org/10.1116/1.579607.
[36] R. Hielscher, H. Schaeben, D. Chateigner, On the entropy to texture index relationship in quantitative texture analysis, J. Appl. Crystallogr. 40 (2007) 371–375, https://doi.org/10.1107/S0021889806055476.
[37] M. Saleem, L. Fang, A. Wakeel, M. Rashad, C.Y. Kong, Simple preparation and characterization of nano-crystalline zinc oxide thin films by sol-gel method on glass substrate, World J. Condens. Matter Phys. 2 (2012) 10–15, https://doi.org/10.4236/wjcmp.2012.21002.
[38] A. Ismail, M.J. Abdullah, The structural and optical properties of ZnO thin films prepared at different RF sputtering power, J. King Saud Univ. Sci. 25 (2013) 209–215, https://doi.org/10.1016/j.jksus.2012.12.004.
[39] Z.-Y. Ye, H.-L. Lu, Y. Geng, Y.-Z. Gu, Z.-Y. Xie, Y. Zhang, Q.-Q. Sun, S.-J. Ding, D.W. Zhang, Structural, electrical, and optical properties of Ti-doped ZnO films fabricated by atomic layer deposition, Nanoscale Res. Lett. 8 (2013) 108, https://doi.org/10.1186/1556-276X-8-108.
[40] R. Haarindraprasad, U. Hashim, S.C.B. Gopinath, M. Kashif, P. Veeradasan, S.R. Balakrishnan, K.L. Foo, P. Poopalan, Y.K. Mishra, Low temperature annealed zinc oxide nanostructured thin film-based transducers: characterization for sensing applications, PloS One (2015), https://doi.org/10.1371/journal.pone.0132755.
[41] A.F. Abdulrahman, S.M. Ahmed, M.A. Almessiere, Effect of the growth time on the optical properties of ZnO nanorods grown by low temperature method, Dig. J. Nanomater. Biostructures. 12 (2017) 1001–1009.
[42] B.D. Viezbicke, S. Patel, B.E. Davis, D.P. Birnie, Evaluation of the Tauc method for optical absorption edge determination: ZnO thin films as a model system, Phys. Status Solidi Basic Res. 252 (2015) 1700–1710, https://doi.org/10.1002/pssb.201552007.
[43] O. Lupan, T. Pauporté, L. Chow, B. Viana, F. Pellé, L.K. Ono, B. Roldan Cuenya, H. Heinrich, Effects of annealing on properties of ZnO thin films prepared by electrochemical deposition in chloride medium, Appl. Surf. Sci. 256 (2010) 1895–1907, https://doi.org/10.1016/j.apsusc.2009.10.032.
[44] Y. Tak, D. Park, K. Yong, Characterization of ZnO nanorod arrays fabricated on Si wafers using a low-temperature synthesis method, J. Vac. Sci. Technol. B Microelectron. Nanom. Struct. 24 (2006) 2047–2883, https://doi.org/10.1116/1.2216714.
[45] S. Bang, S. Lee, J. Park, S. Park, Y. Ko, C. Choi, H. Chang, H. Park, H. Jeon, The effects of post-annealing on the performance of ZnO thin film transistors, Thin Solid Films 519 (2011) 8109–8113, https://doi.org/10.1016/J.TSF.2011.05.048.
[46] Y.J. Kim, H.J. Kim, Trapped oxygen in the grain boundaries of ZnO polycrystalline thin films prepared by plasma-enhanced chemical vapor deposition, Mater. Lett. 41 (1999) 159–163, https://doi.org/10.1016/S0167-577X(99)00124-X.
[47] E. Guziewicz, M. Godlewski, L. Wachnicki, T.A. Krajewski, G. Luka, S. Gieraltowska, R. Jakiela, A. Stonert, W. Lisowski, M. Krawczyk, J.W. Sobczak, A. Jablonski, ALD grown zinc oxide with controllable electrical properties, Semicond, Sci. Technol. 27 (2012), 074011, https://doi.org/10.1088/0268-1242/27/7/074011.
[48] Y.F. Sun, S.B. Liu, F.L. Meng, J.Y. Liu, Z. Jin, L.T. Kong, J.H. Liu, Metal oxide nanostructures and their gas sensing properties: a review, Sensors 41 (2012) 159–163, https://doi.org/10.3390/s120302610.
[49] K. Ellmer, Resistivity of polycrystalline zinc oxide films: current status and physical limit, J. Phys. D Appl. Phys. 34 (2001) 3097–3108, https://doi.org/10.1088/0022-3727/34/21/301.
[50] L. Fanni, B.A. Aebersold, D.T.L. Alexander, L. Ding, M. Morales Masis, S. Nicolay, C. Ballif, c-texture versus a-texture low pressure metalorganic chemical vapor deposition ZnO films: lower resistivity despite smaller grain size, Thin Solid Films 565 (2014) 1–6, https://doi.org/10.1016/J.TSF.2014.06.033.
[51] J. Steinhauser, S. Faÿ, N. Oliveira, E. Vallat-Sauvain, C. Ballif, Transition between grain boundary and intragrain scattering transport mechanisms in boron-doped zinc oxide thin films, Appl. Phys. Lett. 90 (2007) 142107, https://doi.org/10.1063/1.2719158.
[52] F. Werner, Hall measurements on low-mobility thin films, J. Appl. Phys. 122 (2017) 135306, https://doi.org/10.1063/1.4990470.
[53] T.S. Bjørheim, E. Kotomin, Ab initio thermodynamics of oxygen vacancies and zinc interstitials in ZnO, J. Phys. Chem. Lett. 5 (2014) 4238–4242, https://doi.org/10.1021/jz5018812.
[54] J.W. Orton, M.J. Powell, The hall effect in polycrystalline and powdered semiconductors, Rep. Prog. Phys. 43 (1980) 1263, https://doi.org/10.1088/0034-4885/43/11/001.
[55] F. Greuter, G. Blatter, Electrical properties of grain boundaries in polycrystalline compound semiconductors, Semicond. Sci. Technol. 5 (1990) 111–137, https://doi.org/10.1109/TNS.2004.832574.
[56] N. Barsan, U. Weimar, Conduction model of metal oxide gas sensors, J. Electroceram. 7 (2001) 143–167, https://doi.org/10.1023/A:1014405811371.
[57] A. Varpula, J. Sinkkonen, S. Novikov, Modelling of dc characteristics for granular semiconductors, Phys. Scr., T T141 (2010), 014003, https://doi.org/10.1088/0031-8949/2010/T141/014003.
[58] P. Gorai, E.G. Seebauer, E. Ertekin, Mechanism and energetics of O and O_2 adsorption on polar and non-polar ZnO surfaces, J. Chem. Phys. 144 (2016) 184708, https://doi.org/10.1063/1.4948939.
[59] W. Göpel, Reactions of oxygen with ZnO–10$\bar{1}$0-surfaces, J. Vac. Sci. Technol. 15 (2002) 1298–1310, https://doi.org/10.1116/1.569757.
[60] A.B. Djurišić, Y.H. Leung, K.H. Tam, Y.F. Hsu, L. Ding, W.K. Ge, Y.C. Zhong, K.S. Wong, W.K. Chan, H.L. Tam, K.W. Cheah, W.M. Kwok, D.L. Phillips, Defect emissions in ZnO nanostructures, Nanotechnology 18 (2007), 095702, https://doi.org/10.1088/0957-4484/18/9/095702.
[61] B. Panigrahy, M. Aslam, D.S. Misra, M. Ghosh, D. Bahadur, Defect-related emissions and magnetization properties of ZnO Nanorods, Adv. Funct. Mater. 20 (2010) 1161–1165, https://doi.org/10.1002/adfm.200902018.
[62] H. Morkoç, Ü. Özgür, Zinc Oxide: Fundamentals, Materials and Device Technology, 2009, https://doi.org/10.1002/9783527623945.
[63] B.J. Jin, S. Im, S.Y. Lee, Violet and UV luminescence emitted from ZnO thin films grown on sapphire by pulsed laser deposition, Thin Solid Films 366 (2000) 107–110, https://doi.org/10.1016/S0040-6090(00)00746-X.

[64] T. Singh, T. Lehnen, T. Leuning, D. Sahu, S. Mathur, Thickness dependence of optoelectronic properties in ALD grown ZnO thin films, Appl. Surf. Sci. 289 (2014) 27–32, https://doi.org/10.1016/j.apsusc.2013.10.071.
[65] I. Łukasiewicz, A. Wójcik-Godowska, E. Guziewicz, A. Wolska, T. Klepka, P. Dłuewski, R. Jakieła, E. Łusakowska, K. Kopalko, W. Paszkowicz, Wachnicki, S. Witkowski, W. Lisowski, M. Krawczyk, J.W. Sobczak, A. Jabłoński, M. Godlewski, ZnO, ZnMnO and ZnCoO films grown by atomic layer deposition, Semicond. Sci. Technol. 27 (2012), 074009, https://doi.org/10.1088/0268-1242/27/7/074009.
[66] P.X. Gao, Z.L. Wang, Substrate atomic-termination-induced anisotropic growth of ZnO nanowires/nanorods by the VLS process, J. Phys. Chem. B 108 (2004) 7534–7537, https://doi.org/10.1021/jp049657n.
[67] M.A. Rueter, J.M. Vohs, The surface reactions of ethyl groups on Si(100) formed via dissociation of adsorbed diethylzinc, Surf. Sci. 262 (1992) 42–50, https://doi.org/10.1016/0039-6028(92)90458-I.
[68] H. Dumont, A. Marbeuf, J.E. Bourée, O. Gorochov, Mass-spectrometric study of thermal decomposition of diethylzinc and diethyltellurium, J. Mater. Chem. 2 (1992) 923–930, https://doi.org/10.1039/JM9920200923.
[69] G. Fan, N. Maung, T.L. Ng, J.O. Williams, A.C. Wright, Homogeneous thermal decomposition of dimethylzinc in a metal-organic vapour phase epitaxy reactor, J. Chem. Soc. Faraday. Trans. 91 (1995) 3475–3479, https://doi.org/10.1039/FT9959103475.
[70] G. Kresse, O. Dulub, U. Diebold, Competing stabilization mechanism for the polar ZnO(0001)-Zn surface, Phys. Rev. B Condens. Matter 68 (2003) 1–15, https://doi.org/10.1103/PhysRevB.68.245409.
[71] B. Meyer, First-principles study of the polar O-terminated ZnO surface in thermodynamic equilibrium with oxygen and hydrogen, Phys. Rev. B Condens. Matter 69 (2004) 1–10, https://doi.org/10.1103/PhysRevB.69.045416.
[72] R. Wahl, J.V. Lauritsen, F. Besenbacher, G. Kresse, Stabilization mechanism for the polar ZnO(000$\bar{1}$)-O surface, Phys. Rev. B Condens. Matter 87 (2013) 1–12, https://doi.org/10.1103/PhysRevB.87.085313.
[73] O. Dulub, U. Diebold, G. Kresse, Novel stabilization mechanism on polar surfaces: ZnO(0001)-Zn, Phys. Rev. Lett. 90 (2003), 016102, https://doi.org/10.1103/PhysRevLett.90.016102.
[74] L. Bengtsson, Dipole correction for surface supercell calculations, Phys. Rev. B Condens. Matter 59 (1999) 12301, https://doi.org/10.1103/PhysRevB.59.12301.
[75] R.M. Martin, Comment on calculations of electric polarization in crystals, Phys. Rev. B 9 (1974) 1998, https://doi.org/10.1103/PhysRevB.9.1998.